

# Residual Stress Distribution in a Functionally Graded Alumina-Silicon Carbide Material

C.E.J. Dancer<sup>1\*</sup>, M. Achintha<sup>2</sup>, C.J. Salter<sup>1</sup>, J.A. Fernie<sup>1,3</sup> and R.I. Todd<sup>1</sup>

<sup>1</sup> Department of Materials, University of Oxford, Parks Road, Oxford, OX1 3PH, UK

<sup>2</sup> Department of Engineering Science, University of Oxford, Parks Road, Oxford, OX1 3PJ, UK

<sup>3</sup> Ceramics Joining Limited, Tidmarsh House, Tidmarsh, Reading, RG8 8HA

\* Corresponding author. Email: claire.dancer@materials.ox.ac.uk

## Abstract

Functionally graded ceramic structures have a range of potential applications as they enable the exploitation of two ceramic materials with very different properties, such as coefficient of thermal expansion. We report the microstructural investigation of a novel functionally graded structure for alumina and silicon carbide with systematically varied composition. Stresses in the structure have been modelled analytically and by finite element modelling, and are consistent with fluorescence microscopy measurements of residual stress in the structure.

## Keywords

Functionally Graded Materials; Ceramics; Residual Stresses.

Functionally graded materials (FGMs) possess a systematically varied microstructure and/or composition resulting in gradual changes in their mechanical, physical and/or chemical properties across the geometry [1]. FGMs have been proposed as an interlayer for joining dissimilar materials (both ceramic-ceramic and ceramic-metal couples), as they potentially reduce the residual stresses caused by the mismatch in coefficients of thermal expansion (CTE) [2,3] and the large temperature changes in the manufacturing process.

In this work we investigate the microstructure in a ceramic FGM cylinder with composition which changes semi-continuously from SiC-rich at one end to Al<sub>2</sub>O<sub>3</sub>-rich at the other. By this we mean that the FGM is made up of individual layers with each adjacent layer having a slightly different composition such that at one end it is predominantly SiC, and at the other predominantly Al<sub>2</sub>O<sub>3</sub>. The CTEs of SiC and Al<sub>2</sub>O<sub>3</sub> are significantly different at  $4.7 \times 10^{-6} \text{ }^{\circ}\text{C}^{-1}$  for SiC (for temperatures 0-1700°C) and  $8.6 \times 10^{-6} \text{ }^{\circ}\text{C}^{-1}$  for Al<sub>2</sub>O<sub>3</sub> (for 0-1727°C) [4]. The number and thickness of the individual layers must be chosen to keep the generated residual stresses within acceptable limits and so avoid cracking. We then use experimental measurements along with finite element and analytical models to determine the residual stresses developed in the cylinder.

The production of slab-like SiC/C ceramic FGMs [5] and Al<sub>2</sub>O<sub>3</sub>-Si<sub>3</sub>N<sub>4</sub> graded structures [6] have previously been reported, but Al<sub>2</sub>O<sub>3</sub>-SiC FGMs have not been described before to our knowledge. The cylindrical FGM in our work had diameter and length of 20mm and individual layers in the final structure were approximately 2.2mm thick, which is within the range suggested for ceramic-metal FGM structures of similar dimensions [7]. The layers

were assembled using submicron powders mixed in suitable proportions, and hot pressed under uniaxial load at temperatures up to 1800°C in an inert atmosphere.

SiC is typically processed using sintering aids consisting of a combination of aluminium, boron and carbon (or compounds of these) [8-10] which lower the sintering temperature to 1850-2100°C, while maintaining good mechanical properties [11]. However for this assembly it is critical that the sintering temperature is below 1850°C in order to prevent excessive grain growth of alumina at the alumina-rich end of the structure. In addition, the integrity of the FGM will be affected by the thermal expansion mismatch between SiC and Al<sub>2</sub>O<sub>3</sub>, which will become larger if cooling is from higher temperatures.

An alternative route is to use a combination of oxide phases as liquid-phase sintering aids [8,12] ("LPS SiC"). The literature shows that the highest density SiC at the lowest sintering temperature was obtained by Sciti and Bellosi using hot pressing, by adding a mixture of 4wt.% Y<sub>2</sub>O<sub>3</sub> and 6wt.% Al<sub>2</sub>O<sub>3</sub> to 90wt% SiC powder [8] at 1800°C and 30MPa pressure, which had density above 98% of the theoretical maximum. This composition was therefore chosen for the SiC-rich end of the FGM.

The processing requirements for densification of monolithic Al<sub>2</sub>O<sub>3</sub> are well established [13]. Ultra-high purity Al<sub>2</sub>O<sub>3</sub> can be fully densified without abnormal grain growth (AGG) [13,14]. However low levels of MgO is often added to avoid AGG and increase strength [13,15], as AGG caused by slight contamination of the starting powder is common [16]. Dense Al<sub>2</sub>O<sub>3</sub> with small grain size can be produced by hot pressing alumina powder with 0.25wt.% MgO in flowing argon at temperatures of 1470-1650°C and under 25 MPa uniaxial pressure [17]. However, higher temperatures were required here to fully densify the SiC-rich end of the FGM, which could result in a large grain size and decreased strength at the Al<sub>2</sub>O<sub>3</sub>-rich end. Therefore, the final layer of the FGM had composition 10wt.% SiC-Al<sub>2</sub>O<sub>3</sub>.

The intermediate layers of this FGM have systematically varying Al<sub>2</sub>O<sub>3</sub> and SiC content. Dense SiC-Al<sub>2</sub>O<sub>3</sub> composites with up to 30vol.% Al<sub>2</sub>O<sub>3</sub> content have been produced by a number of researchers [18-21]. While these compositions are now well-established, we are unaware of any research reported in the literature on the production of Al<sub>2</sub>O<sub>3</sub>-SiC composites containing 40-80% SiC by powder processing. Yang and Troczynski [22] used sol-gel processing and pressureless sintering to produce Al<sub>2</sub>O<sub>3</sub>-SiC composites with up to 60vol.% SiC content but this method is not completely suitable for the production of FGM structures due to the high shrinkage during processing and relatively high residual porosity [22].

The composition used for the SiC-richest layer was modified for 40-80% SiC compositions. In the SiC-richest layer, under appropriate heat-treatment conditions, Y<sub>2</sub>O<sub>3</sub> and Al<sub>2</sub>O<sub>3</sub> powders form a liquid sintering aid [23]. The presence of YAG was confirmed by X-ray diffraction (not shown) of discs with the SiC-rich compositions. The Y<sub>2</sub>O<sub>3</sub> and Al<sub>2</sub>O<sub>3</sub> contents were linearly decreased from the amount added to the SiC-richest layer to zero for the 30% SiC layer.

Fig. 1a shows a typical FGM assembly consisting of 9 layers. The cylinder was sectioned lengthways using a diamond blade, mounted in resin and polished (Fig. 1b). Microstructural analyses were carried out in order to understand the compositional variations and residual stresses within the FGM.

Examination of the polished cross-section by optical microscopy revealed no macroscopic cracking. Some porosity was evident at the boundary between the 80 and 90% SiC layers. Further investigations were made using a field-emission scanning electron microscope (JEOL 6500F) in back-scattered mode (Fig. 2). The Al<sub>2</sub>O<sub>3</sub>-rich end (Fig. 2a) contains submicron SiC particles (grey) in an Al<sub>2</sub>O<sub>3</sub> matrix (lighter) and with limited fine scale porosity (black). The Al<sub>2</sub>O<sub>3</sub> grain size is 3-5µm. The microstructure at the centre of the rod (Fig. 2b) was similar to the Al<sub>2</sub>O<sub>3</sub>-rich end, with more SiC and slightly more residual porosity. The white regions are mainly YAG originating from the liquid phase. Interfaces were confirmed to be crack-free and relatively sharp.

The 80% SiC layer showed unusual “fern-like” features close to the interface with the 90% SiC layer (Fig. 2c) over ~100µm regions orientated approximately perpendicular to the interface. The strong atomic number contrast of the features indicates that some flow and segregation of the YAG liquid phase occurred during sintering, possibly driven by capillary forces resulting from regions of different density. The microstructure within the rest of the SiC-rich end (Fig. 2d) contains some small inhomogeneous regions. Areas which were richer in liquid have sintered well and conversely the regions that are deficient in liquid show some fine scale porosity. Similar segregation has been observed in LPS SiC densified by FAST/SPS and was attributed to the formation of large YAG crystals during cooling [24].

To study the residual stresses in the FGM, fluorescence microscopy experiments were performed on the cross-section using a confocal Raman microscope (System 1000, Renishaw, UK) with a motorised stage and incident radiation from a 633 nm He-Ne laser (50x lens, spatial resolution ~5µm). The position of the R1 fluorescence peak (associated with Cr<sup>3+</sup> impurities [25]) was measured every 0.25mm along the length of the rod and repeated 3 times along different lines (Fig. 3). This wavelength is related to the mean stress ( $\sigma_m$ ) by Eq. (1), where  $\Delta\nu$  is the change in wavenumber and  $\bar{\Pi}_m$  is the mean piezospectroscopic coefficient (7.59cm<sup>-1</sup>GPa<sup>-1</sup> for polycrystalline alumina) [26].

$$\Delta\nu = \bar{\Pi}_m \sigma_m \quad (1)$$

In the 7<sup>th</sup> layer of the sample (70% SiC) the Al<sub>2</sub>O<sub>3</sub>/Cr<sup>3+</sup> fluorescence signal became too weak to measure accurately owing to the diminishing amount of alumina. However observations on the alumina-rich end enable us to assess the general trend in the residual stress. The good agreement between the three separate line scans shows the reproducibility of the technique and the uniformity of the stresses in the rod.

There are two main sources of residual stress in the FGM structure: the thermal expansion mismatch between Al<sub>2</sub>O<sub>3</sub> and SiC in the individual composite layers (“microstresses”), and the mismatch between the layers. Both contribute to shifts in fluorescence peak position. At the Al<sub>2</sub>O<sub>3</sub>-rich end, the microstresses caused by the CTE mismatch between SiC and Al<sub>2</sub>O<sub>3</sub> during cooling can be modelled as an assembly of spherical SiC particles, each surrounded by a concentric spherical shell of alumina with radius chosen to give the correct volume fraction of each component. This has been used previously to understand residual stresses in non-FGM sections of similar composites [19,27]. The volume-averaged mean stress in the alumina,  $\sigma_A$ , can then be assessed [27]:

$$\sigma_A = \frac{fE_A E_S (\alpha_A - \alpha_S) \Delta T}{(1-f)E_A (1-2\nu_S) + E_S [f(1-2\nu_A) + \frac{1}{2}(1+\nu_A)]} \quad (2)$$

where subscripts *A* and *S* refer to the alumina and SiC respectively, *E* is Young's modulus,  $\nu$  is Poisson's ratio, *f* is the volume fraction of SiC,  $\alpha$  is linear thermal expansion coefficient, and  $\Delta T$  is the temperature drop over which the stresses have not been relaxed (*e.g.* by diffusion).

Eq. (2) indicates that the microstresses in the Al<sub>2</sub>O<sub>3</sub> are expected to increase as more SiC is added. Using material property data from Todd *et al* [27] and  $\bar{\Pi}_m$  as given above allows the predicted peak shift for the microstresses alone to be calculated using Eq.s (1) and (2). Previous work [19, 28] shows that the instrument used mainly samples the bulk stresses in materials such as these where one phase is transparent. These are plotted compared with the fluorescence line scan results (Fig. 3) using the nominal midpoints of the layers on the abscissa. The R1 wavenumber is taken as 14404cm<sup>-1</sup> at the centre of the Al<sub>2</sub>O<sub>3</sub>-richest layer, and the reasonable value of 1000°C was assumed for  $\Delta T$ . The agreement is good, showing that the large steps in fluorescent wavelength between layers are due primarily to the microstresses, rather than larger stresses due to the FGM layers. Although the microstresses are large (*e.g.*  $\sigma_A \sim 800$ MPa in the 50% SiC layer), they do not cause cracking because they act over short distances. Previous work has shown that the addition of SiC particles to Al<sub>2</sub>O<sub>3</sub> does not cause cracking until the SiC particles are larger than 10μm [20]; these particles are much smaller ( $\sim 0.5\mu\text{m}$ ) than this critical size.

As the steps observed between layers in Fig. 3 are evidently primarily attributable to the difference in interphase microstresses within each layer, the stresses resulting from mismatches between layers of the FGM are expected to be relatively small. The average Cr<sup>3+</sup> R1 fluorescence peak shift across each layer is  $0.24 \pm 0.09 \text{cm}^{-1}$  corresponding to a mean stress of  $32 \pm 10 \text{MPa}$  from Eq. (1). To examine this further, a commercial FE package (ABAQUS) was also used to determine the distribution of stresses (Fig.4). Axi-symmetric elements were used to model the cylinder and a constant average CTE for each layer was determined by a rule of mixtures method. The residual stresses generated due to mismatch in CTEs at the interfaces between adjacent layers were determined. The results show the residual stresses generated due to the CTE mismatch between the adjacent layers. It should be noted that the elastic mismatch between adjacent layers was small, so the elastic constants were assumed to be the same in all layers. The cylinder is free from external stresses so no boundary restraints are applied in the FE analysis. Fig. 4a-b show that the significant stresses (both radial and hoop directions) developed in the vicinity of the interfaces away from the surface diminish quite rapidly away from them. As expected, the results show no significant longitudinal stresses since the cylinder is free to contract along its axis. A maximum mean stress of about 115MPa is seen close to the axis of the cylinder (Fig. 4c-d). The mean stresses closer to the surface of the cylinder have a lower magnitude than those a small distance below the surface or near the centre (Fig.4d). Near the surface the total change in stress for each layer is  $34 \pm 2 \text{MPa}$ , which is close to the experimental result for the surface stress obtained from fluorescence microscopy (32MPa). Comparing Fig. 3 and Fig. 4d it is apparent that the residual stress measurements obtained from fluorescence microscopy at the surface are

consistent with both the microstresses and surface FGM stresses predicted by the appropriate models.

In summary, we have investigated an alumina-silicon carbide functionally-graded assembly with systematically varied composition. Microstructural characterisation of the structure reveals defect- and crack-free interfaces, apart from the 80-90% SiC interface where some residual porosity is evident. Finite element and analytical microstress models are consistent with surface stresses measured by Cr<sup>3+</sup> fluorescence microscopy.

The authors gratefully acknowledge funding and assistance from TWI (Granta Park, Abington, Cambridge, UK).

- [1] N. Calis, S.R. Kushan, F. Kara, H. Mandal, J. Euro. Ceram. Soc. 24 (2004) 3387.
- [2] J.A. Fernie, P.L. Threadgill, M.N. Watson, Weld. Met. Fabr. 59 (1991) 179.
- [3] C.S. Lee, S.H. Ahn, L.C. DeJonghe, G. Thomas Mat. Sci. Eng. A 434 (2006) 160.
- [4] J.F. Shackelford and W. Alexander (Eds.), CRC Materials Science and Engineering Handbook, CRC Press, Boca Raton, USA, 2001.
- [5] C. Kawai, S. Wakamatsu J. Mater. Sci. Lett. 14 (1995) 467.
- [6] C.S. Lee, X.F. Zhang, G. Thomas Acta Materialia 49 (2001) 3775.
- [7] M. Ito, N. Ishida US Patent No. 4723862 (1988)
- [8] D. Sciti, A. Bellosi J. Mater. Sci. 35 (2000) 3849.
- [9] T. Kinoshita, S. Munekawa, S. Tanaka Acta Materialia 45 (1997) 801.
- [10] J.A. Coppola, N. Hailey, C.H. McMurty US Patent No. 4346049 (1982).
- [11] J.J. Kim J. Mater. Sci. Lett. 15 (1996) 1754.
- [12] F. K. van Dijen, E. Mayer J. Euro. Ceram. Soc. 16 (1996) 413.
- [13] R.L. Coble US Patent No. 3026210 (1962).
- [14] S.I. Bae, S. Baik J. Mater. Sci. 28 (1993) 4197.
- [15] M.N. Rahaman Sintering of Ceramics CRC Press, Boca Raton, USA, 2008.
- [16] W. Jo, D.Y. Kim, N.M. Hwang J. Am. Ceram. Soc. 89 (2006) 2369.
- [17] J.L. Ortiz-Merino, R.I. Todd Acta Materialia 53 (2005) 3345.
- [18] Niihara, K J. Ceram. Soc. Jpn. 99 (1991) 974-982.
- [19] J.L. Ortiz-Merino, R.I. Todd J. Eur. Ceram. Soc. 23 (2003) 1779.
- [20] R.I. Todd, B. Derby Acta Materialia 52 (2004) 1621
- [21] A.M. Cock, I.P. Shapiro, R.I. Todd, S.G. Roberts J. Am. Ceram. Soc. 88 (2005) 2354.
- [22] Q.Z. Yang, T. Troczynski J. Am. Ceram. Soc. 83 (2000) 958.
- [23] E.M. Levin, C.R. Robbins, H.F. McMurdie, Phase diagrams for ceramists American Ceramic Society, Columbus, Ohio, 1969.
- [24] M. Herrmann, R. Neher, K. Brandt, S Hoehn J. Euro. Ceram. Soc 30 (2010) 1495.
- [25] Q. Ma, D.R. Clarke J. Am. Ceram. Soc. 76 (2005) 1433.
- [26] J. He, D.R. Clarke J. Am. Ceram. Soc. 78 (1995) 1347.
- [27] R.I. Todd, M.A.M. Bourke, C.E. Borsa, R.J. Brook Acta Materialia 45 (1997) 1791.
- [28] R.I. Todd, A.R. Boccaccini, R. Sinclair, R.B. Yaltee, R.J. Young Acta Mater. 47 (1999) 3233.

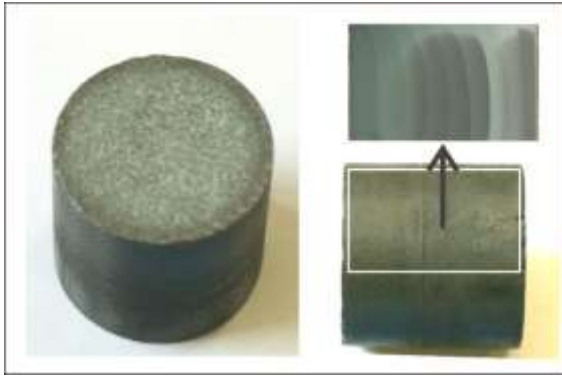


Figure 1: As-sintered FGM cylinder and polished cross-section showing layered structure.

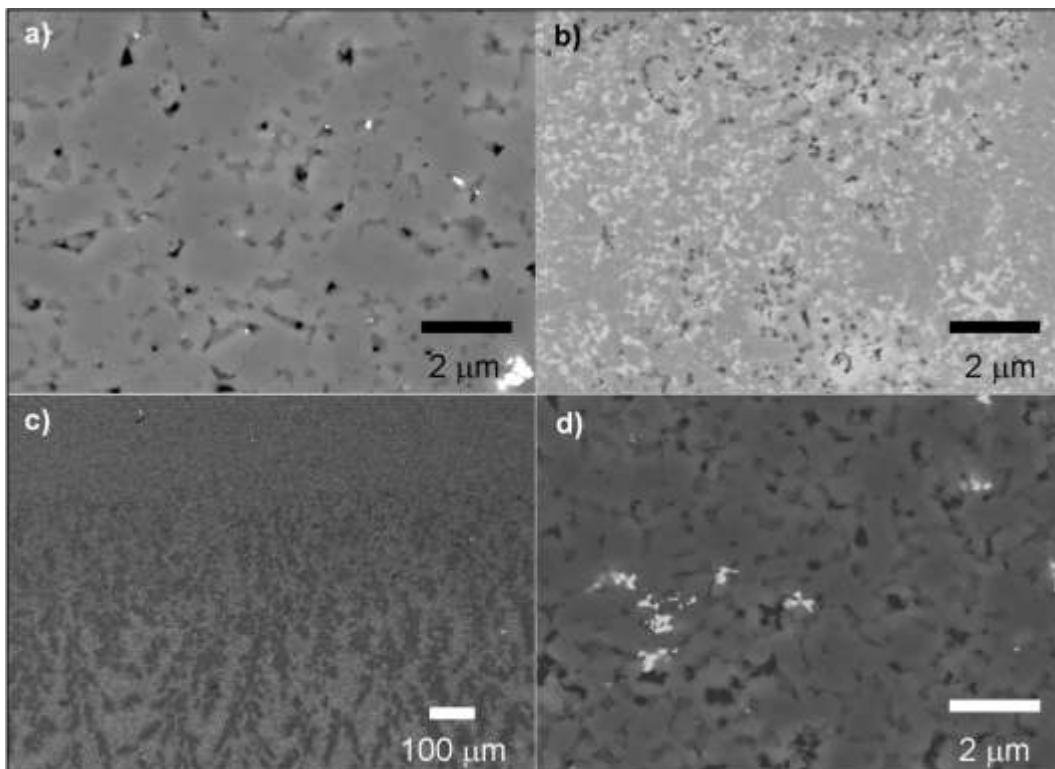


Figure 2: Back-scattered scanning electron microscope images of regions of interest a) alumina-rich end b) centre of the FGM c) interface between 80%-90% SiC layers d) SiC-rich end.

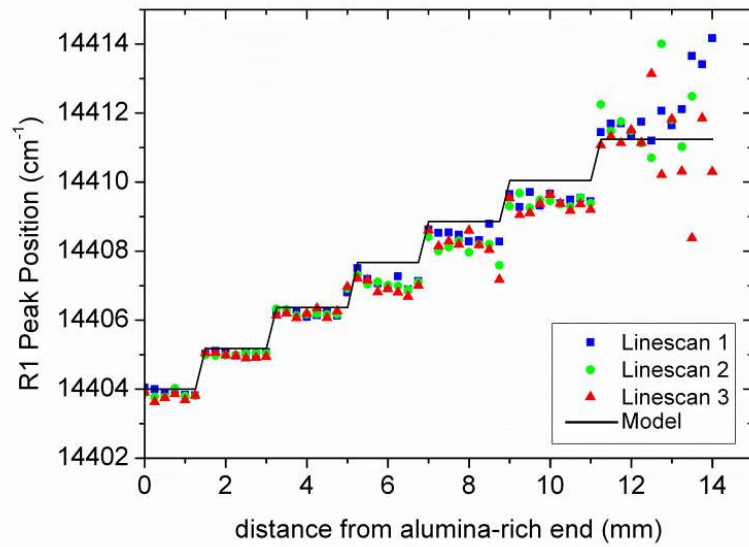


Figure 3: Model for interphase stresses and experimental data for  $\text{Cr}^{3+}$  fluorescence R1 peak position as function of distance along the FGM from the alumina-rich end.

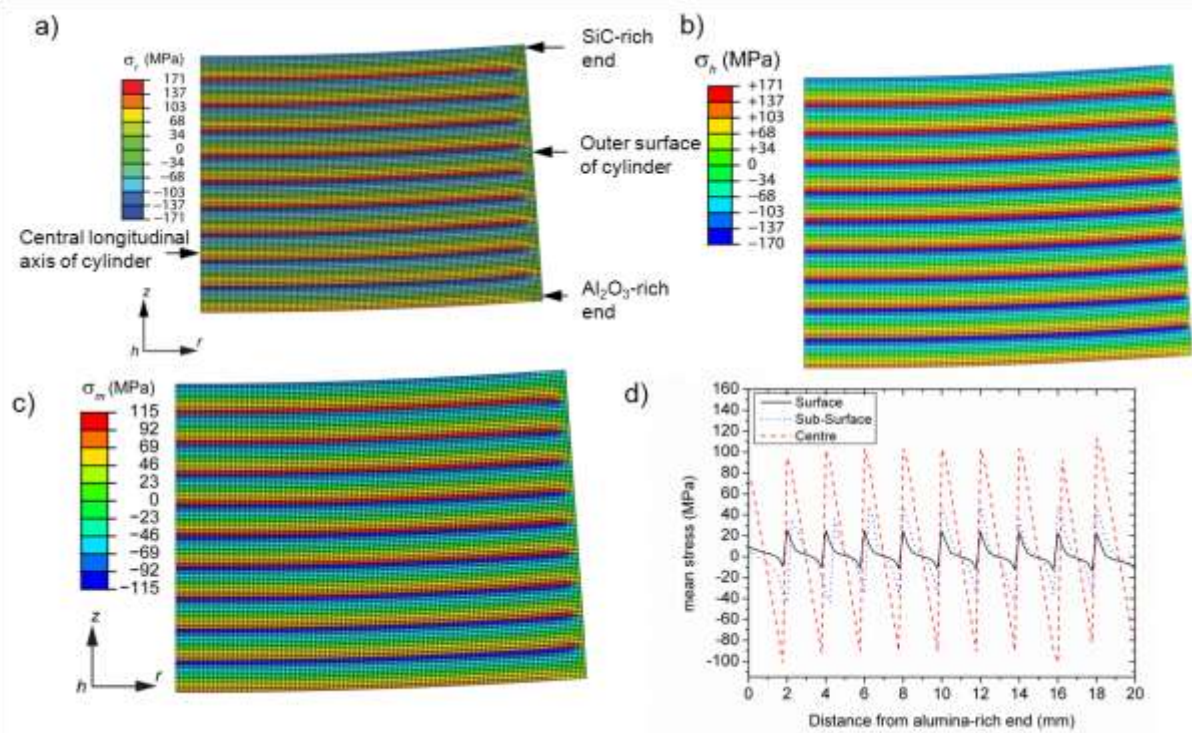


Figure 4: Finite element modelling of residual stresses in a FGM cylinder. a) Radial stress b) hoop stress, c) mean stress, d) line-scan of mean stress along the longitudinal axis of the cylinder at positions  $\sim 0.2$  mm ("Surface") and  $\sim 0.8$  mm ("Sub-Surface") from the outer surface, and at the central axis of the cylinder ("Centre").